



# **Radiological Dose Calculations for the Chamber and Diode Region of the Light Ion Fusion Target Development Facility**

**O. Yasar, M.E. Sawan, D.L. Henderson, G.A. Moses**

**July 1987**

**UWFDM-726**

***FUSION TECHNOLOGY INSTITUTE  
UNIVERSITY OF WISCONSIN  
MADISON WISCONSIN***

### **DISCLAIMER**

This report was prepared as an account of work sponsored by an agency of the United States Government. Neither the United States Government, nor any agency thereof, nor any of their employees, makes any warranty, express or implied, or assumes any legal liability or responsibility for the accuracy, completeness, or usefulness of any information, apparatus, product, or process disclosed, or represents that its use would not infringe privately owned rights. Reference herein to any specific commercial product, process, or service by trade name, trademark, manufacturer, or otherwise, does not necessarily constitute or imply its endorsement, recommendation, or favoring by the United States Government or any agency thereof. The views and opinions of authors expressed herein do not necessarily state or reflect those of the United States Government or any agency thereof.

**Radiological Dose Calculations for the  
Chamber and Diode Region of the Light Ion  
Fusion Target Development Facility**

O. Yasar, M.E. Sawan, D.L. Henderson, G.A.  
Moses

Fusion Technology Institute  
University of Wisconsin  
1500 Engineering Drive  
Madison, WI 53706

<http://fti.neep.wisc.edu>

July 1987

UWFDM-726

**RADIOLOGICAL DOSE CALCULATIONS FOR THE CHAMBER AND DIODE REGION  
OF THE LIGHT ION FUSION TARGET DEVELOPMENT FACILITY**

*O. Yasar*

*M.E. Sawan*

*D.L. Henderson*

*G.A. Moses*

Fusion Technology Institute  
1500 Johnson Drive  
University of Wisconsin-Madison  
Madison, Wisconsin 53706

July 1987

UWFDM-726

## ABSTRACT

Biological dose rate calculations have been performed for the Light Ion Fusion Target Development Facility (TDF) for times following an operational period of one month. The primary wall material considered is aluminum Al-6061-T6 with an alternative material being 2-1/4 Cr-1 Mo steel. The diode material considered is SS304LN stainless steel and the penetration in the chamber wall is 10 cm in radius. As an alternative to the base case 3 m radius chamber design, a 1 m radius chamber is analyzed with various shield materials -- borated water, concrete and graphite between the chamber wall and the diode. The dose rate behind the Al first wall for the 3 m chamber design is 34.5 mrem/hr at 1 week after shutdown. For the 1 m chamber design this number is 8.4 rem/hr with an aluminum first wall, and 5 rem/hr with a steel first wall.

For the diode region calculations the first wall is taken as Al-6061-T6 for both the 1 m and 3 m cases. The dose rate at a point external to the diode vacuum casing, one week after shutdown, is 24.5 mrem/hr for the 3 m case. For the 1 m case, the dose rates at one week after shutdown are 3.7, 3.83 and 5.8 mrem/hr with shield materials of borated water, concrete and graphite.

## 1. INTRODUCTION

The Light Ion Beam Target Development Facility (TDF) is a proposed experimental facility intended to test high gain ICF targets. During its peak operation period, the facility is to test 50-800 MJ fusion targets at the rate of 10 to 12 per day, accumulating approximately 15,000 shots over a five year time period. Activation of the target debris, target chamber and surrounding components occurs as the high energy neutrons released by the initiation and subsequent burn of the DT fuel interact with the materials. Being an experimental device, the level of radioactivity induced by this number of high yield shots is of concern as access to the target chamber, the ion diodes and a target diagnostic package may be required relatively soon after a shot or a number of shots.

The preliminary design of TDF uses aluminum 6061-T6 as the chamber wall material and has the target explosion chamber submerged in a borated water pool as portrayed in Fig. 1a. As an alternative to this 3 m radius chamber design, a 1 m radius chamber with two different first wall materials -- Al-6061-T6 and 2-1/4 Cr-1 Mo steel -- is examined. This is shown in Fig. 1b. The biological dose rates behind the first wall are compared for these wall materials. The 3 m chamber design is also examined with a few changes from our previous studies.<sup>(1)</sup> In particular, the boron in the borated water pool surrounding the chamber is enriched to 90% boron-10 for neutron absorbing purposes. Also the 100 cm thick graphite moderator (40% void fraction) is replaced by 49 cm of graphite (no void). The dose rate at 1 week after shutdown behind the wall is increased from 25 mrem/hr<sup>(1)</sup> to 35 mrem/hr due to less graphite.

As a critical part of the TDF design, the high voltage diodes, which convert the electrical pulse into beams, are subject to neutron activation that can lead to high dose levels in their vicinity which influence the maintenance schedule. The dose rates are calculated at a point external to the diode casing. The ion diode material considered is stainless steel SS304LN and the penetration opening through the first wall to the diode is considered as 10 cm in radius. A schematic of a TDF diode is shown in Fig. 2.

The dose rates in the diode region are calculated for both the 3 m and the 1 m chamber designs. The first wall material is taken as Al-6061-T6. Compared to the 3 m case, the 1 m chamber leaves room between the first wall and diode for shielding the diode region. Shielding materials considered are borated water, concrete and graphite. Among them, borated water shielding gives preferable results. The dose rate behind the first wall in the 1 m chamber is significantly greater than the 3 m chamber but the dose rate at the diode is less. This sets up a trade-off between early access to the chamber or to the diodes.

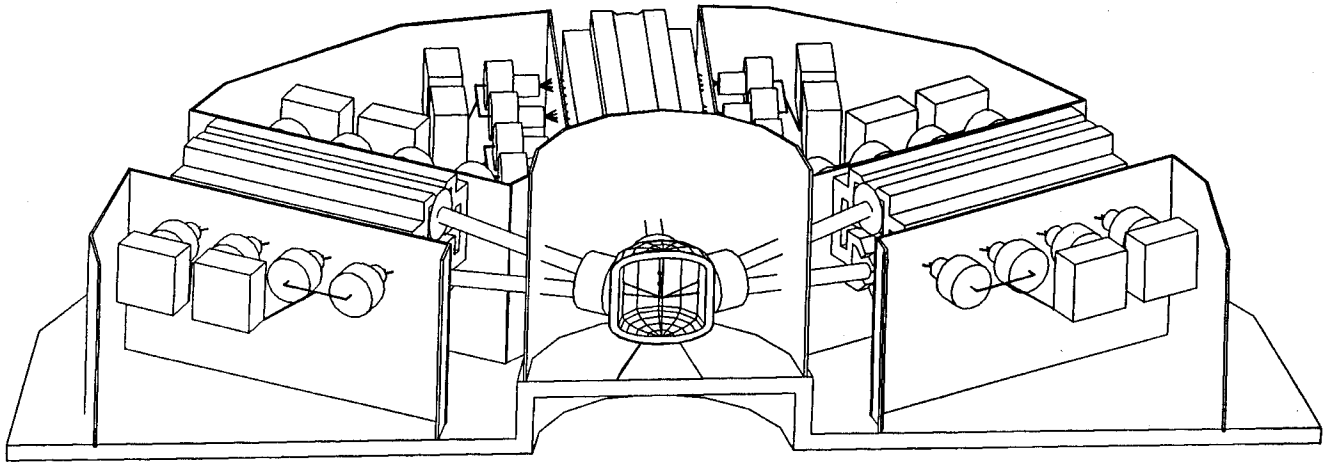


**Fig. 1a. Preliminary design of the Light Ion Fusion Target Development Facility.**

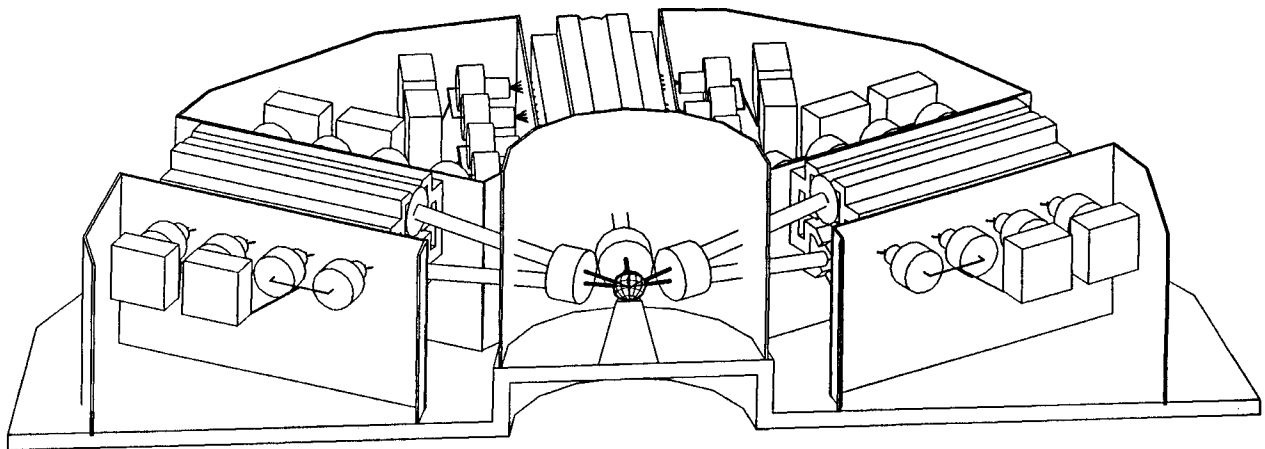


**Fig. 1b. TDF chamber design with 1 m radius chamber.**

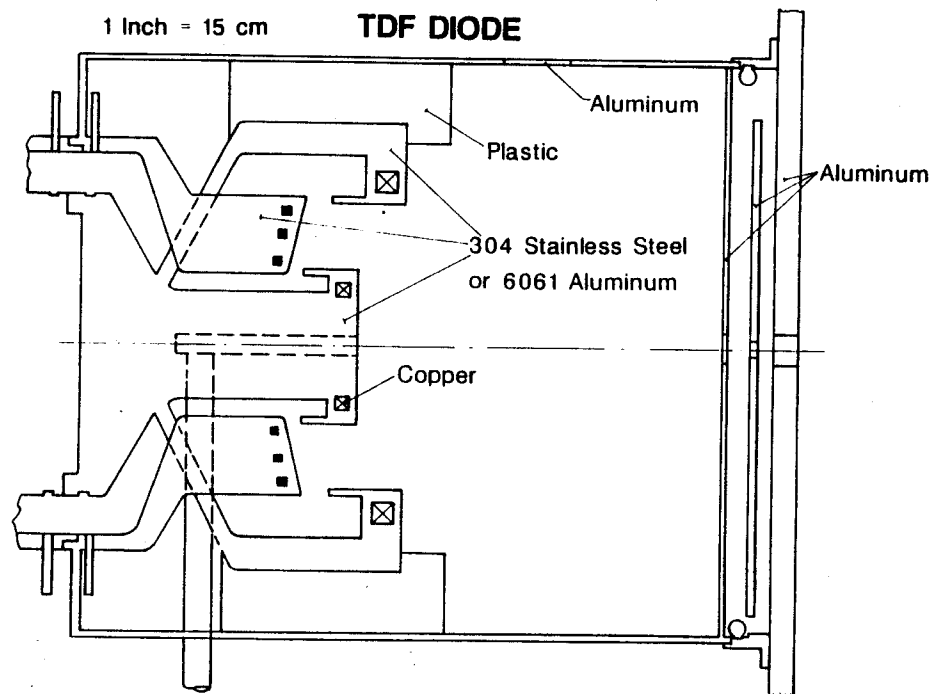


Fig. 2. Schematic of the high voltage ion diode used for the neutronic and dose rate calculations.

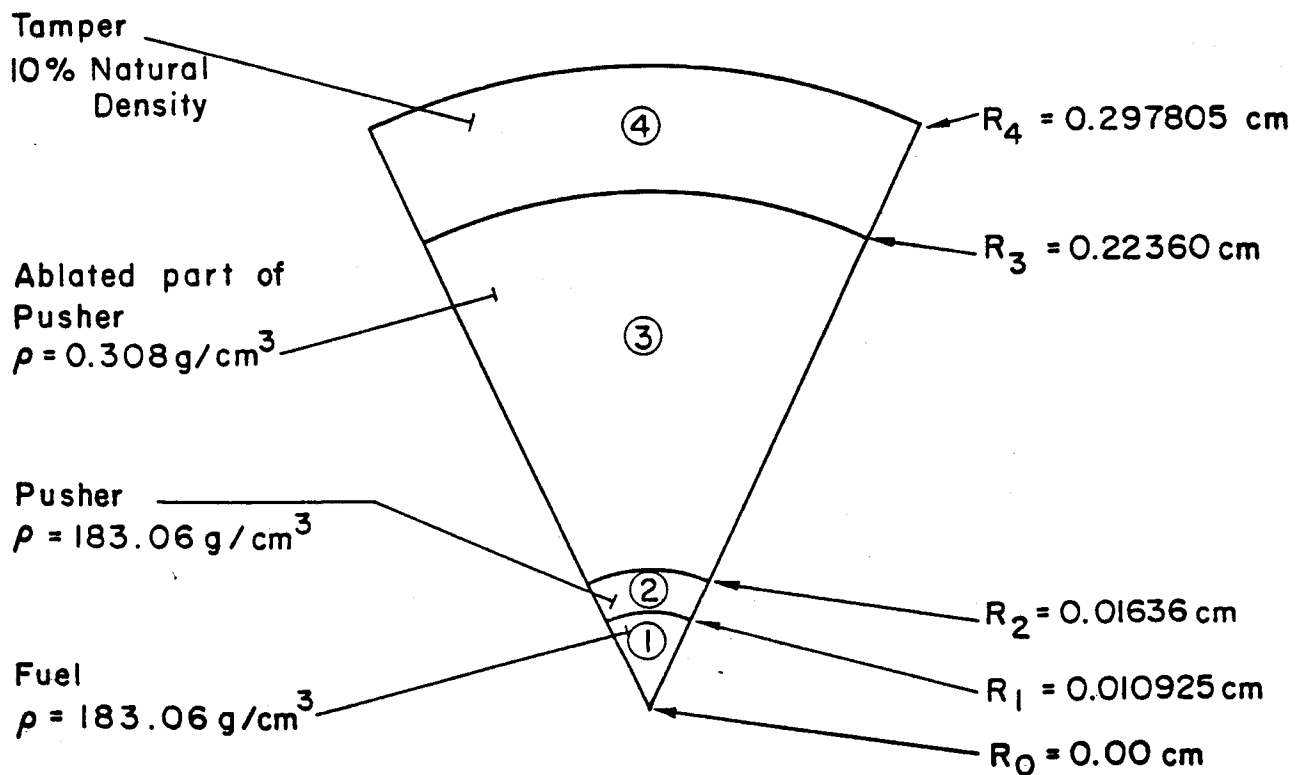


Fig. 3. The compressed target configuration used in the target neutronics calculations.



A brief description of the data libraries and codes used in the neutronics calculations is given in Section 2. Also contained therein are the calculational model and procedure for the computations. Section 3 contains a description of the data libraries and codes used in the radioactivity and dose rate calculations. This is followed by the dose rate results in Section 4.

## 2. NEUTRON TRANSPORT CALCULATIONS

A consistent neutronics analysis must account for neutron target interactions which result in considerable spectrum softening of the fusion neutrons. The target DT load was assumed to be 1 mg and the fuel was assumed to be compressed to a density times radius product ( $\rho R$  value) of  $2 \text{ g/cm}^2$ . The compressed target configuration used in the neutron transport calculations is shown in Fig. 3. A tamper density that is 10% of the natural density was used to account for the effect of heating by the impinging ion beams.

The spectrum of neutrons escaping from the target obtained from the target neutronics calculations is given in Fig. 4. For each D-T fusion, 1.046 neutrons leak from the target. A fuel burnup fraction of 30% was assumed giving approximately 100 MJ of fusion energy released from the 1 mg fuel target used in the calculations. Since the TDF target is required to produce a yield of 200 MJ a D-T mass of 2 mg will be needed. For the same ignition  $\rho R$  value, intrinsic quantities such as neutron spectrum are assumed not to change while absolute quantities such as neutron yield are scaled by a factor of 2. A 200 MJ target D-T yield corresponds to  $7.09 \times 10^{19}$  D-T fusions per shot and  $7.42 \times 10^{19}$  neutrons emanating from the target per shot. The neutron spectrum obtained from the target neutronics calculation was used to represent the source for the chamber neutronics.

The neutron flux in the diode is computed in two steps. First the cylindrically shaped target chamber is approximated by spherical geometry for a one-dimensional calculation. The TDF target chamber models used in the one-dimensional calculations are given in Fig. 5 for the 3 m and 1 m chamber designs. The first wall thickness is increased by 0.5 cm in the calculation model to account for the chamber structural support. The boral layers have boron enriched to 90%  $^{10}\text{B}$ . The source is considered to be a point isotropic source at the center of the cavity. The neutron spectrum obtained from the target neutronics calculation was used to represent the source for the chamber calculation. The one-dimensional discrete ordinates code ONEDANT<sup>(2)</sup> was used together with the LANL MATXS5<sup>(3)</sup> cross section data library processed from the ENDF/B-V evaluated file. The standard LANL 30 neutron-12 gamma group structure was used. The calculations were performed using the  $P_3$ - $S_{16}$  approximation. The neutron

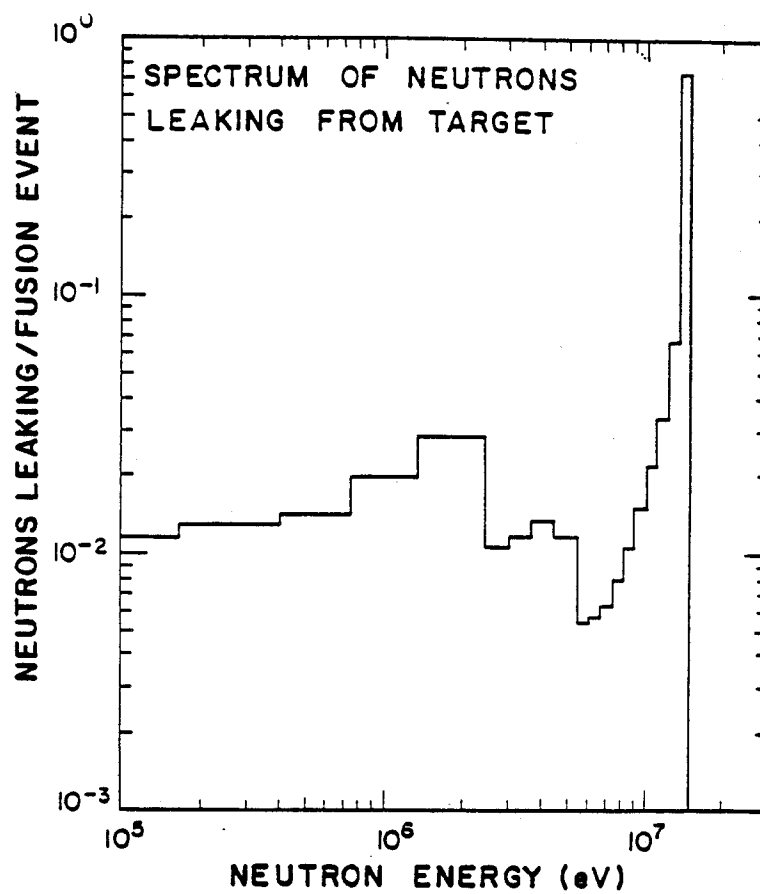


Fig. 4. Spectrum of neutrons emerging from the target.

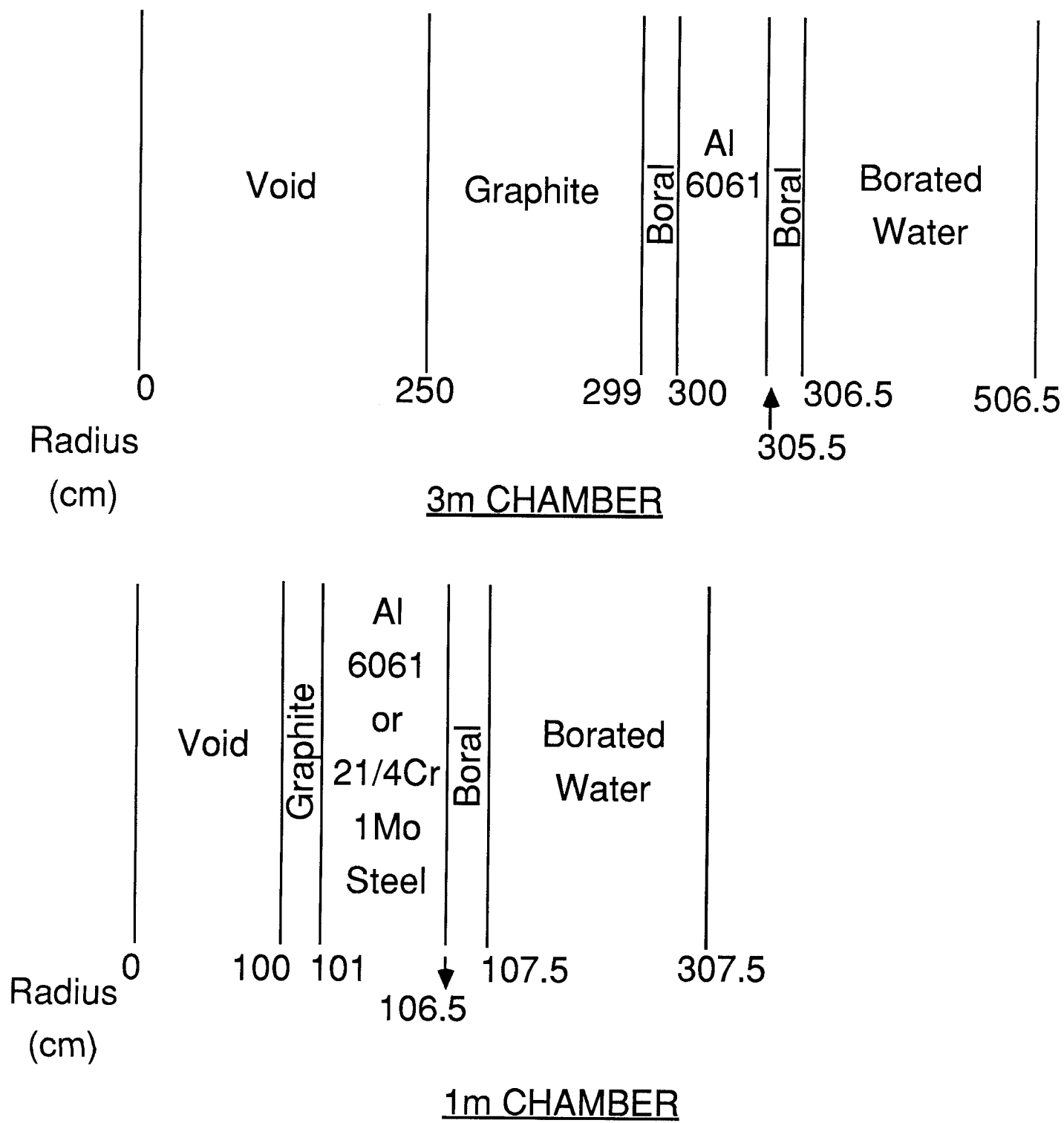


Fig. 5. One-dimensional schematic of the Target Development Facility 1 m chamber design used for the neutronic and activation calculations.

flux obtained from the one-dimensional calculations was used to determine the wall activation and dose at the outer surface of the chamber wall.

The one-dimensional cavity calculation discussed above is used to obtain the energy and angular distribution of neutrons incident on the inner surface of the chamber. These are used to represent a surface source in the second step of the calculation where the detailed geometrical configuration of the diode is modeled. Since the beam ports occupy less than 2% of the inner surface area, the one-dimensional calculation in which the penetrations are not modeled gives a fairly accurate estimate of the nuclear radiation incident on the inner surface of the chamber and the beam penetration opening. In addition, since the diodes are located in the facility midplane, using spherical geometry in the one-dimensional calculation yields reasonably accurate results for nuclear radiation incident on the area around the beam ports.

The energy spectra of neutrons incident on the inner surface of the graphite are shown in Fig. 6 for the different chamber designs considered. The results represent the integral over all directions going into the graphite and are normalized to one D-T fusion and are given per energy group of the 30 neutron-12 gamma standard LANL group structure. Included also for comparison is the spectrum of neutrons emerging from the target. For each D-T fusion in the target, 1.046 neutrons emanate from the target and impinge directly on the inner surface of the chamber. Neutron scattering collisions in the surrounding materials results in reflecting some of these neutrons back into the cavity. These reflected neutrons will end up impinging on the graphite with a fraction of them reflected again into the cavity.

The total number of neutrons incident on the inner surface of the chamber for each DT fusion is 6.929 for the 3 m Al chamber. It is interesting to note that this is slightly higher than that obtained for the previous preliminary design when the inner surface of the graphite was at a smaller radius with scattered neutrons having a smaller probability of reentering the cavity. The corresponding numbers for the 1 m chamber with Al and steel walls are 1.553 and 2.065, respectively. The significantly smaller amount of neutrons reentering the cavity in the 1 m chamber case is related to the smaller cavity radius and less reflection by the thin graphite liner. Only 15% of the total impinging neutrons came directly from the target in the 3 m chamber case resulting in a spectrum that is much softer than that emerging from the target. Harder neutron spectra are obtained in the 1 m chamber case with the uncollided neutrons representing 67% and 50% of the total number of neutrons for the Al and steel walls, respectively. It should be pointed out that the angular distribution of incident neutrons varies from one energy group to the other. Peaking in the normal direction is more pronounced for high energy

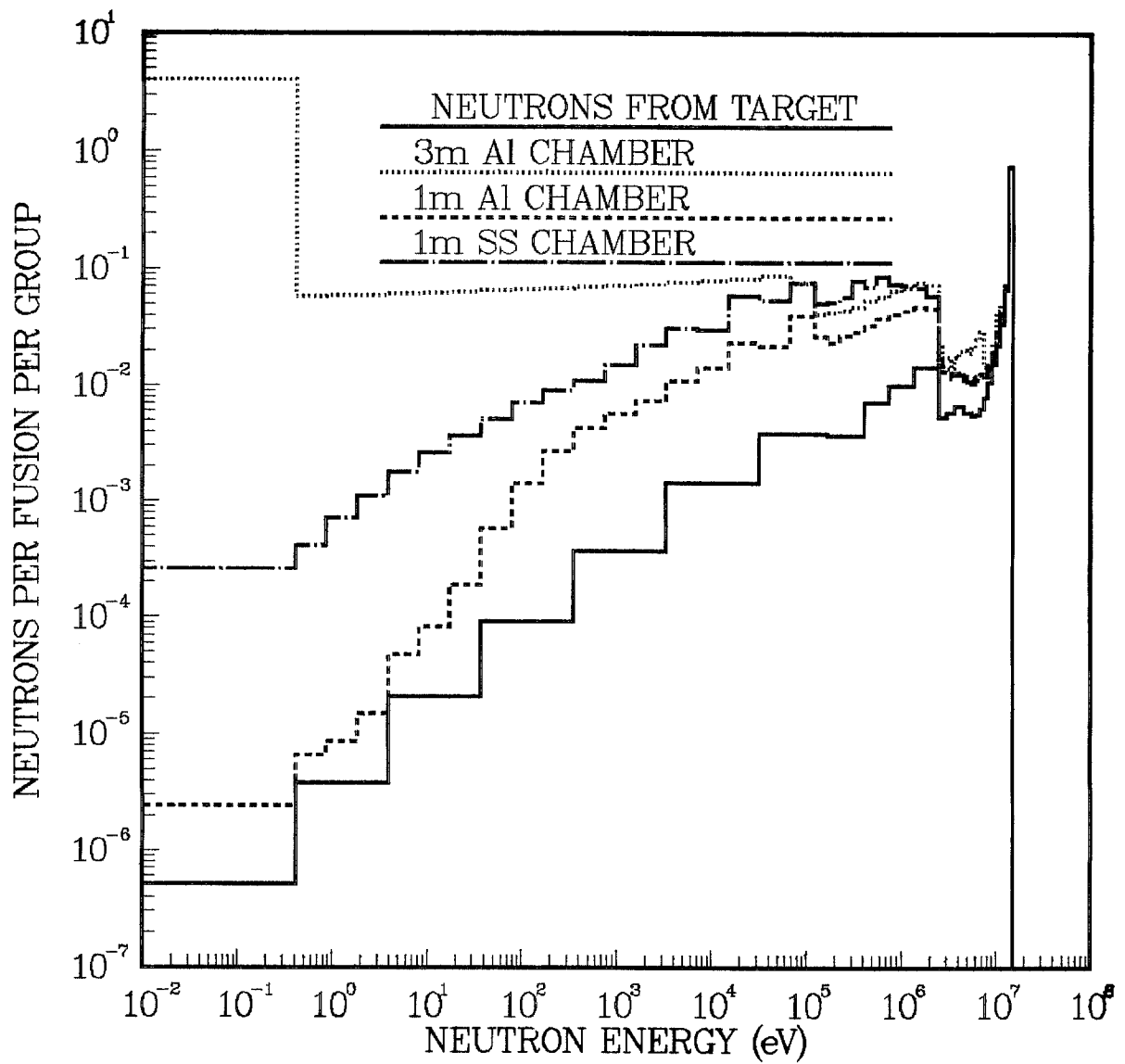


Fig. 6. Energy spectrum of neutrons incident on front surface of graphite in TDF.

groups where the direct contribution from the target is large. The energy spectra of neutrons incident on the liner in the discrete ordinates directions are stored to serve as surface source distributions in the two-dimensional calculation that properly models the detailed diode geometry. A relatively large  $S_N$  order of 16 is used here for proper representation of the angular distribution of neutrons incident on the inner surface of the chamber.

Two-dimensional neutronics calculations have been performed to determine the flux distribution in the diode. The diode geometry was modeled in two-dimensional r-z geometry. Calculations have been performed for both the 3 m and 1 m chamber designs. The cathode and anode are made of stainless steel 304LN and the penetration radius is 10 cm. Three calculations have been performed for the 1 m chamber case with three different shielding materials, namely borated water, concrete, and graphite being used in the space between the first wall and the diode. Hence, a total of four two-dimensional neutronics calculations has been performed. Figs. 7 and 8 give the r-z geometrical models used in the calculations for the 3 m and 1 m chamber cases, respectively.

The two-dimensional discrete ordinates code TWODANT<sup>(4)</sup> was used in the calculations with the same 30 neutron-12 gamma multigroup cross section data based on the ENDF/B-V evaluation which was used in the one-dimensional calculation. A spatially uniform surface source was used at the bottom boundary represented by the energy dependent angular flux at the inner surface of the chamber as obtained from the appropriate one-dimensional calculation. The source is given in the eight discrete ordinates directions going into the graphite region. The source is assumed to be uniform in the azimuthal direction. A vacuum boundary condition is used at the bottom boundary since the contribution from neutrons reentering the cavity from the surrounding materials is already taken into account in the surface source. A vacuum boundary is also used at the top. A right reflecting boundary is used in the calculational model to account for the interaction between adjacent penetrations. This boundary should be located at half the distance between the adjacent penetrations. In the actual geometry this distance increases as one moves from the inner surface of the chamber to the diode. However, the two-dimensional r-z geometry allows only for a cylindrical reflecting boundary as shown in Figs. 6 and 7. Furthermore, while the spacing is smaller at the inner surface of the 1 m chamber than that in the 3 m chamber, it is identical at the diodes which are located at the same distance from the target in both cases. In the 3 m chamber case the reflecting boundary is taken at a radius of 125 cm which is the distance between the penetration centerline and the plane of symmetry between adjacent

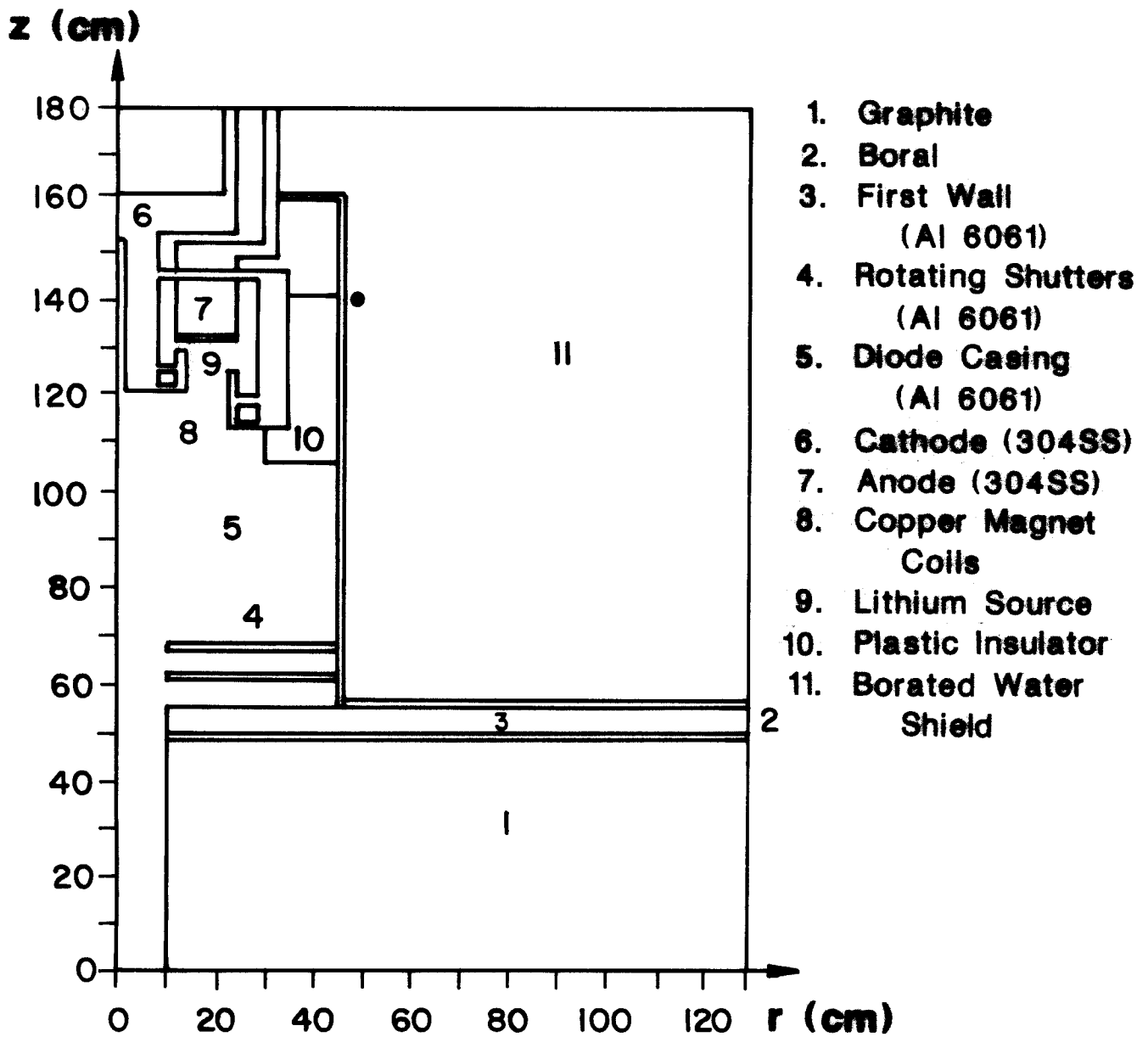


Fig. 7. The r-z geometrical model used in the two-dimensional neutronics and activation calculations for the 3 m chamber design.

penetrations at the inner surface of the graphite region. This is expected to give conservative estimates for the flux in the diode due to the larger shielding space between adjacent diodes. In the 1 m chamber case the distance between the penetration centerline and the plane of symmetry between adjacent penetrations is 50 cm at the inner surface of the graphite liner and increases rapidly to values larger than 125 cm in the diode region. The sensitivity of the calculated flux to the location of the reflecting boundary was determined by performing calculations for reflecting boundaries at radii of 50 and 125 cm. The flux in the 10 cm radius beam duct was found to not be sensitive to the location of the reflecting boundary due to the large shielding space between adjacent penetrations even for the 50 cm radius reflecting boundary. On the other hand, the 50 cm radius reflecting boundary results in overestimating the flux in the diode by up to ~60% since only 8 cm shielding space is provided between adjacent diodes in this case. Since the spacing between diode centerlines is larger than 125 cm in the actual design, a reflecting boundary radius of 125 cm is also used for the 1 m chamber calculational model.

It should be noted that the use of a cylindrical reflecting boundary is equivalent to surrounding the modeled diode by diode penetrations at all azimuthal locations. This tends to overestimate the flux and dose in the diode area. Furthermore, using an r-z model with a planar disc source at the bottom boundary does not take into account the geometrical attenuation of the flux which can be significant particularly for the component coming directly from the target at the center of the cavity. The  $1/R^2$  geometrical attenuation implies an attenuation factor of ~ 12 for the flux as one goes from the front of the graphite liner to the front of the diode for the 1 m chamber. It is clear, therefore, that the geometrical approximations introduced by the two-dimensional model tend to give conservative estimates for the flux and dose in the diode region. The only way to avoid these geometrical modeling deficiencies is to use the Monte Carlo method where the detailed three-dimensional geometry can be modeled. However, the Monte Carlo method is statistical in nature and is not capable of generating accurate estimates for differential quantities such as the neutron energy spectra in optically thin zones which are required for activation and dose calculations.

In addition to the forward neutron transport calculations, adjoint gamma transport calculations were performed for the four cases considered here. In the adjoint calculations, an adjoint source was used on the outer surface of the diode casing with the energy spectrum given by the gamma flux-to-dose conversion factors. The location of the source is taken at the location where the dose after shutdown is calculated. This position outside the diode casing is at a radius of 47 cm and at a distance of 392 cm from



the center of the cavity. These calculations were used to determine the adjoint dose field distribution that is coupled with the decay gamma source to yield the dose at this position for various times after shutdown.

### 3. DOSE RATE CALCULATIONS

#### 3.1 Libraries and Codes

The dose rate calculations were performed using the DKR-ICF<sup>(5)</sup> code package which consists of the radioactivity calculation code DKR, the data handling code CONVERT and the dose rate calculation code DOSE. The spatial models used for radioactivity and dose calculations are identical to the model used for the TWODANT neutronic calculations and are given in Figs. 5, 7, and 8. The large dot drawn in the figures designates the point at which the dose rate is calculated.

ACTLLIB, a decay and neutron transmutation data library based on the evaluated neutron activation cross section library ACTL<sup>(6)</sup>, is used as the primary database for the activation calculations. The neutron transmutation data is given in a 46 group structure format. The decay and gamma source data is taken from the Table of Isotopes<sup>(7)</sup> with the gamma source data being in a 21 group structure format. Appendix A gives the composition of the materials used in the calculations. The radioactivity and dose calculations take 2-5 minutes of Cray-XMP/48 time per case. This is a great advantage for current and future two-dimensional radioactivity and dose calculations compared to previous studies<sup>(8)</sup> that have taken 9-10 hours of Cray-XMP/48 time. Code optimization in the reference to data libraries has resulted in this cost savings.

#### 3.2 Dose Rate Results

The dose rate results are presented for various designs of chamber wall, chamber structure and shielding materials. Results are normalized to 200 MJ of target yield. The operation of the facility is assumed to be 12 shots per day for 5 days per week for 4 weeks, totaling one month of operation.

The dose rates behind the chamber wall due only to the chamber and borated water are given in Fig. 9. At short times after shutdown (up to 1 week) the dose rate behind the aluminum wall for the 1 m case exceeds the stainless steel dose rates. Thereafter, it drops below it up to 10 years. The initial shape of both 1 m curves up to approximately 1 day after shutdown shows the same behavior and is determined by the decay of short-lived isotopes  $^{28}_{13}\text{Al}$ ,  $^{27}_{12}\text{Mg}$  and  $^{26}_{11}\text{Na}$  in aluminum and  $^{28}_{13}\text{Al}$  and  $^{56}_{25}\text{Mn}$  in stainless steel. The large drop in the aluminum dose rate after one day following the shutdown is the result of the decay of  $^{24}_{11}\text{Na}$  which has a half-life of 15 hours. The 3 m chamber with an aluminum first wall has a similar curve to the 1 m case, except the level for the 3 m

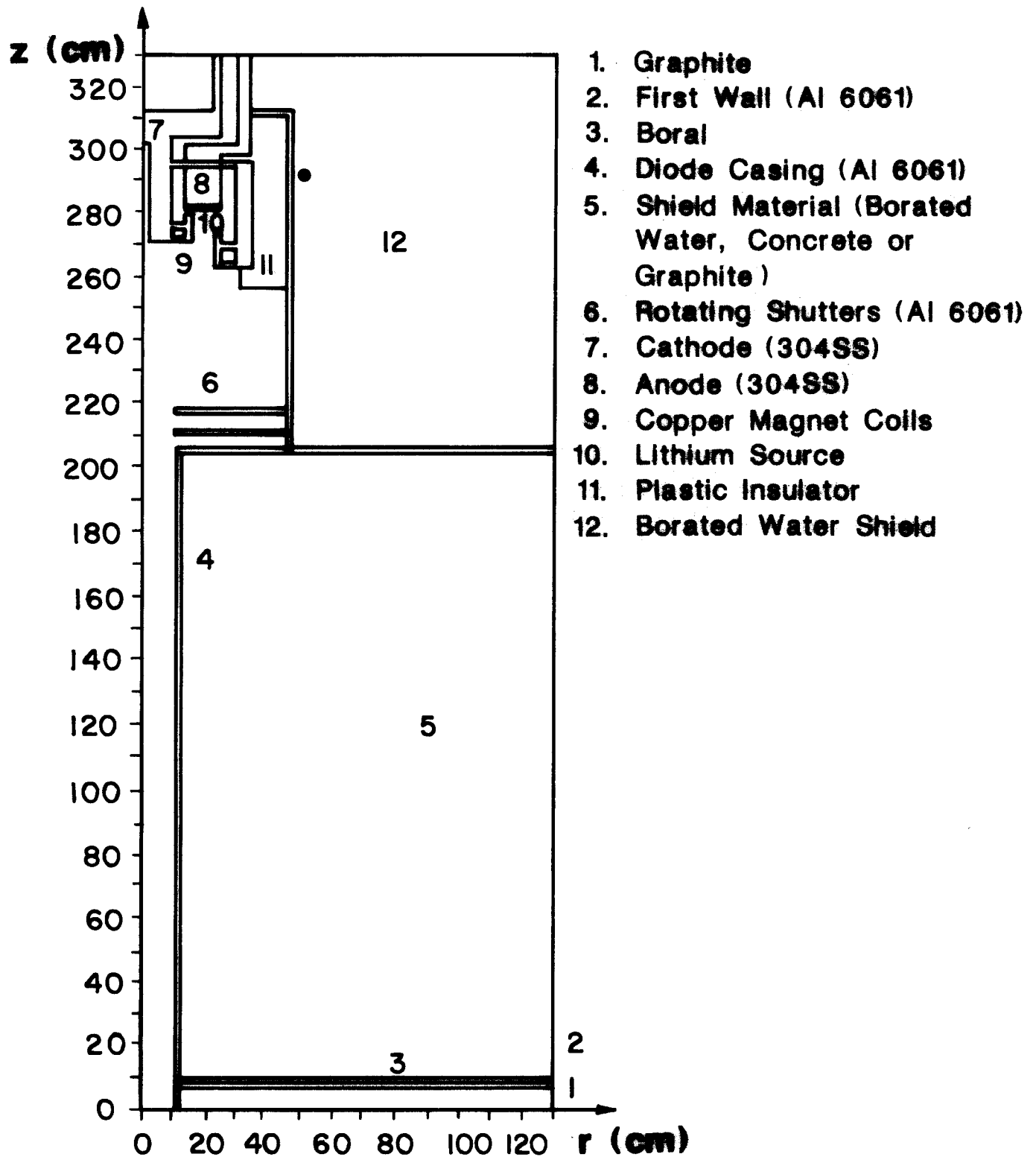


Fig. 8. The r-z geometrical model used in the two-dimensional neutronics and activation calculations for the 1 m chamber design.

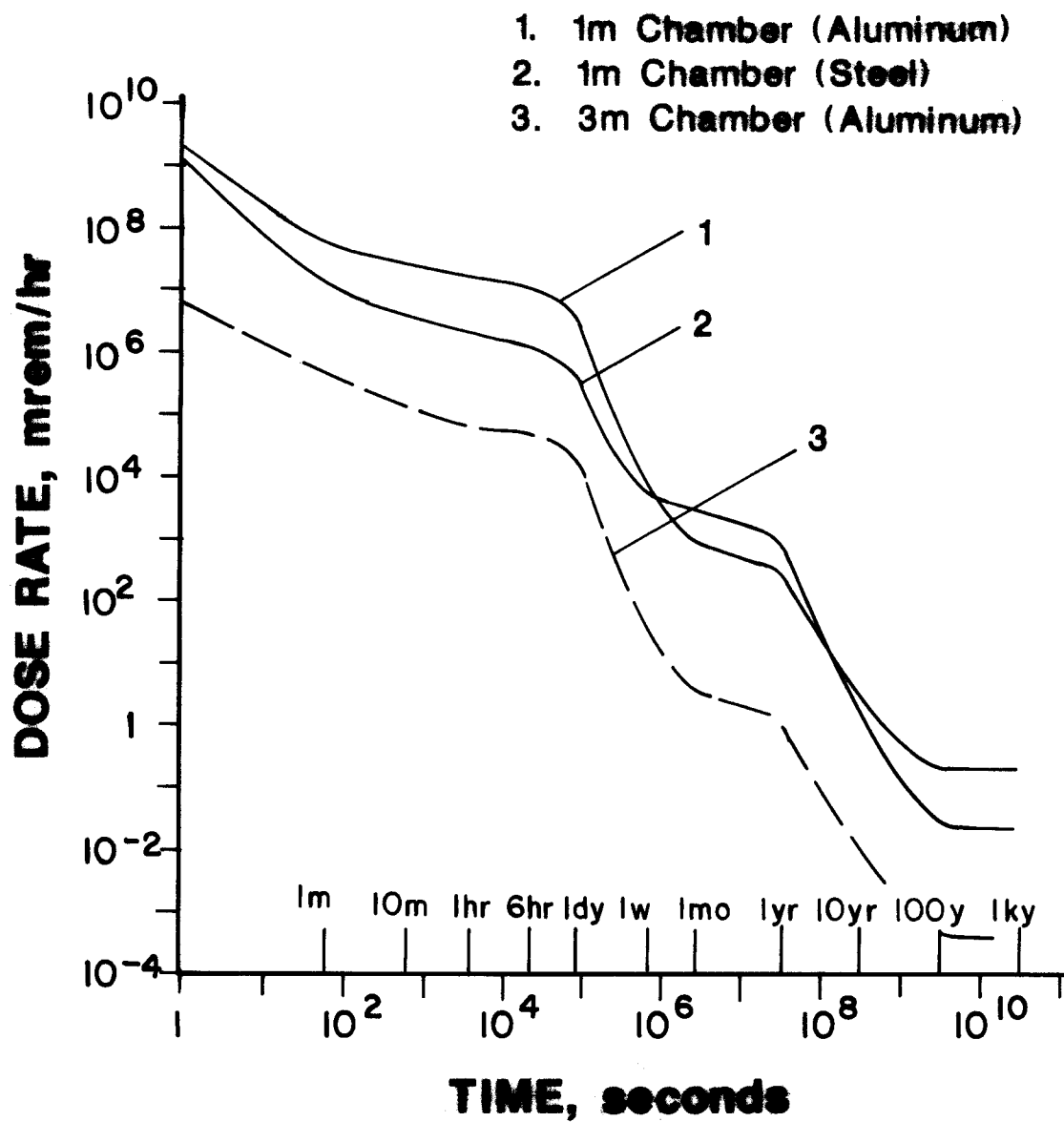


Fig. 9. Dose rates behind the first wall.

case is more than two orders of magnitude lower due to the reduced high energy neutron flux level. This flux has been reduced by the inclusion of 50 cm of graphite within the target chamber.

Figure 10 shows the dose rate results at a position near the diode, as shown in Figs. 7 and 8, for different shielding materials. The dashed line is for the 3 m design and the other three curves are for the 1 m design with various shield materials. The diode material considered is SS304LN stainless steel and the chamber wall material is Al-6061-T6. Among the different shield materials, borated water (with boron enriched to 90%  $^{10}_5\text{B}$ ) is the best for almost all times after shutdown. The lower the level of neutron flux in the diode region, the fewer neutron transmutations that there will be and thus the lower the decay gamma dose level in the system. The dose rate at 1 week after shutdown is 3.7 mrem/hr for the borated water shielding case. The corresponding values for the concrete and graphite shielding cases are 3.83 and 5.8 mrem/hr, respectively.

A comparison is made between the dose rates of the 3 m and 1 m designs and is shown in Fig. 11. When comparing the dose rates behind the aluminum first wall, it is quite clear that the dose for the 1 m chamber wall is much higher, since the 1 m chamber wall is much closer to the target than the 3 m chamber and there is no neutron moderator inside. Due to the higher neutron flux, the number of neutron transmutations and thus the number of gamma producer elements is higher for the 1 m case. The dose rate at 1 week after shutdown is 8.4 rem/hr for the 1 m chamber wall and is 34.5 mrem/hr for the 3 m chamber wall. However, since there is a large shielding space between the 1 m chamber wall and the diode, the dose level at the diode region is lower for the 1 m chamber than the dose level at the diode region for the 3 m chamber. With any shielding material in the 1 m case, the dose rate is in the range of 3-6 mrem/hr at 1 week after shutdown, whereas it is 25 mrem/hr for the 3 m case.

The dose contribution from each component of the system is also of interest. Figures 12 and 13 show the dose rate contribution of each component to the dose rate at the point in the diode region. These components are the aluminum first wall, boral, liner, plastic insulator, copper coils, aluminum casing, shield material and the diode material (SS304LN). As observed from the previous studies,<sup>(8)</sup> the main contribution several days after shutdown comes from just the diode material SS304LN. This is due to long-lived elements  $^{51}_{24}\text{Cr}$ ,  $^{54}_{25}\text{Mn}$ ,  $^{57}_{27}\text{Co}$ ,  $^{58}_{27}\text{Co}$ . On the other hand, the other components such as plastic and borated water, that produce the short-lived element  $^{16}_7\text{N}$  whose half-life is 7.1 seconds, contribute nothing after 4-5 minutes following the shutdown. The components containing a high percent of aluminum (boral, aluminum first wall and casing) follow the same behavior. The drop after 1 day is due to the decay of  $^{24}_{11}\text{Na}$ .

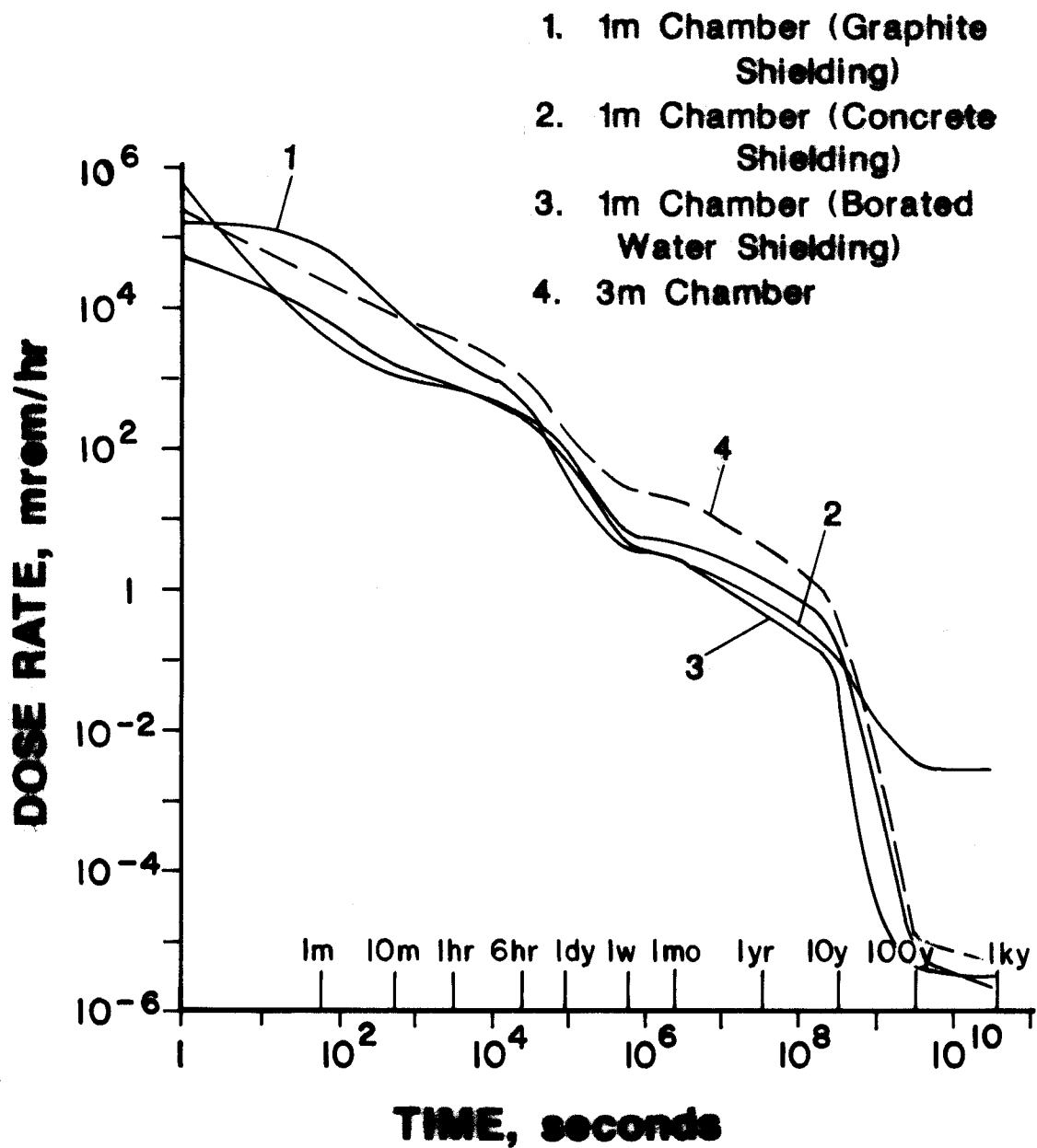


Fig. 10. Dose rates at the diode region for both 1 m and 3 m designs with Al first wall.

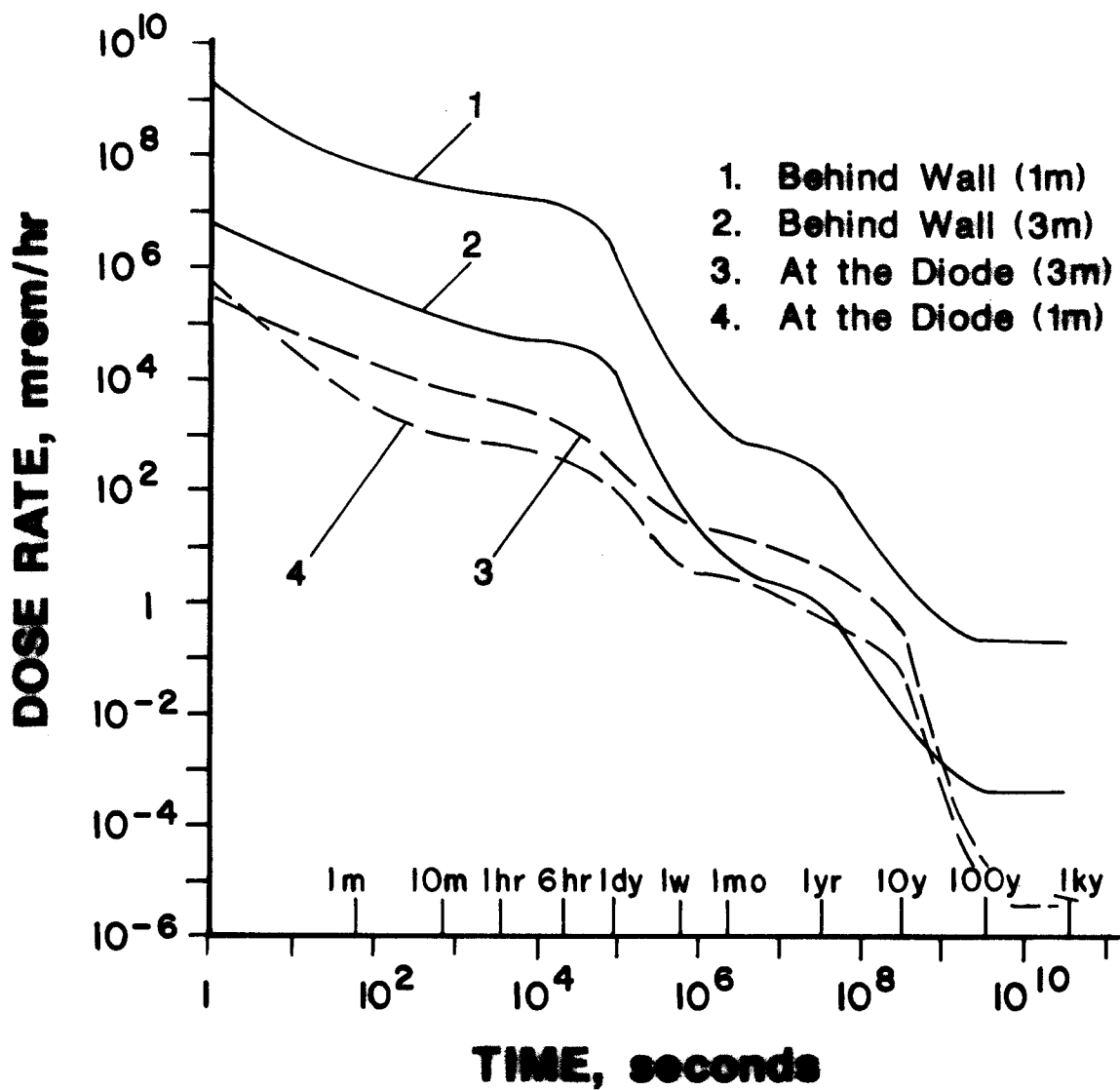


Fig. 11. Chamber wall and diode region dose rate comparison for 1 m and 3 m chamber designs.

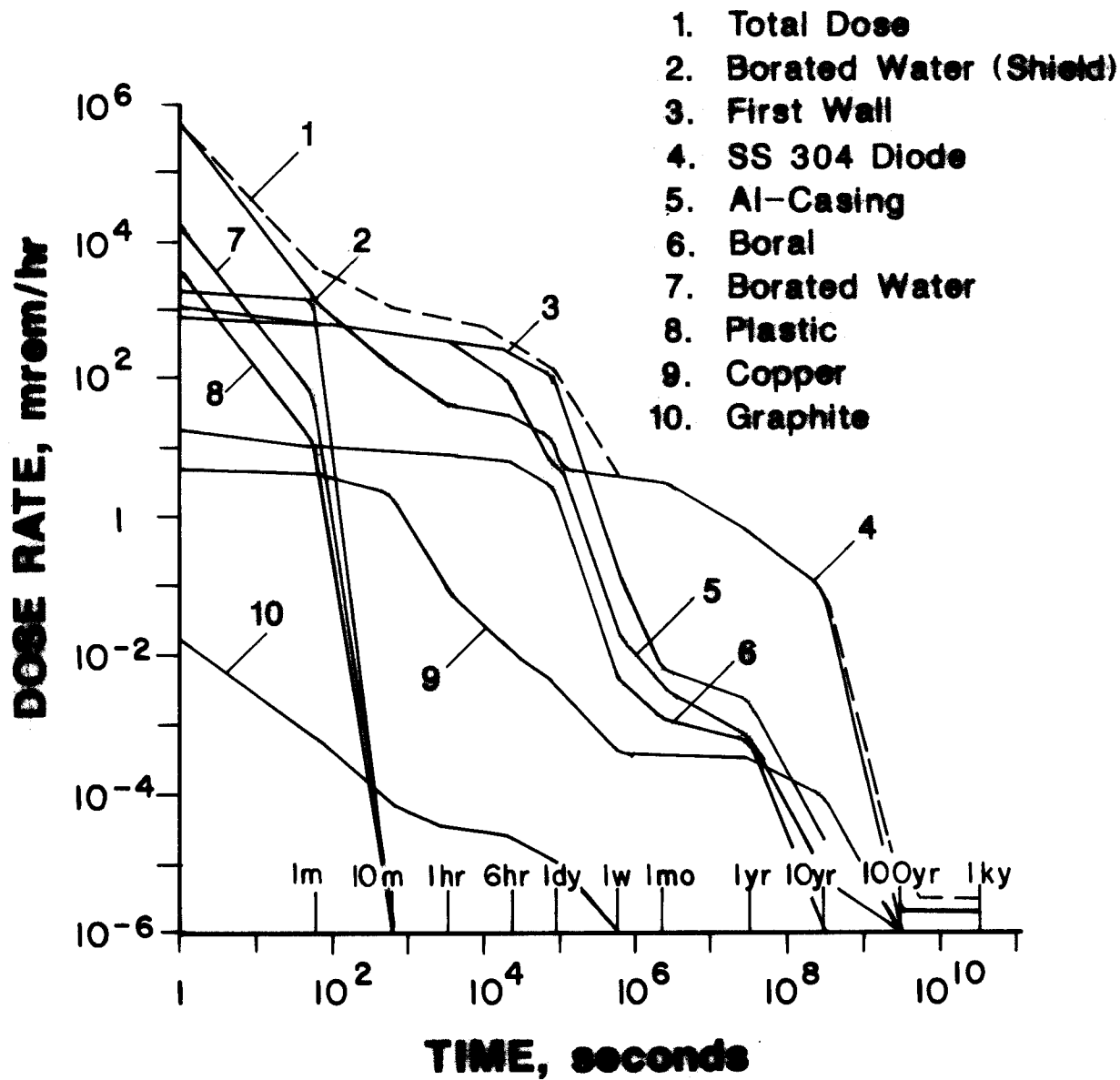


Fig. 12. Contributions from each component to the dose at the diode region for the 1 m chamber design.

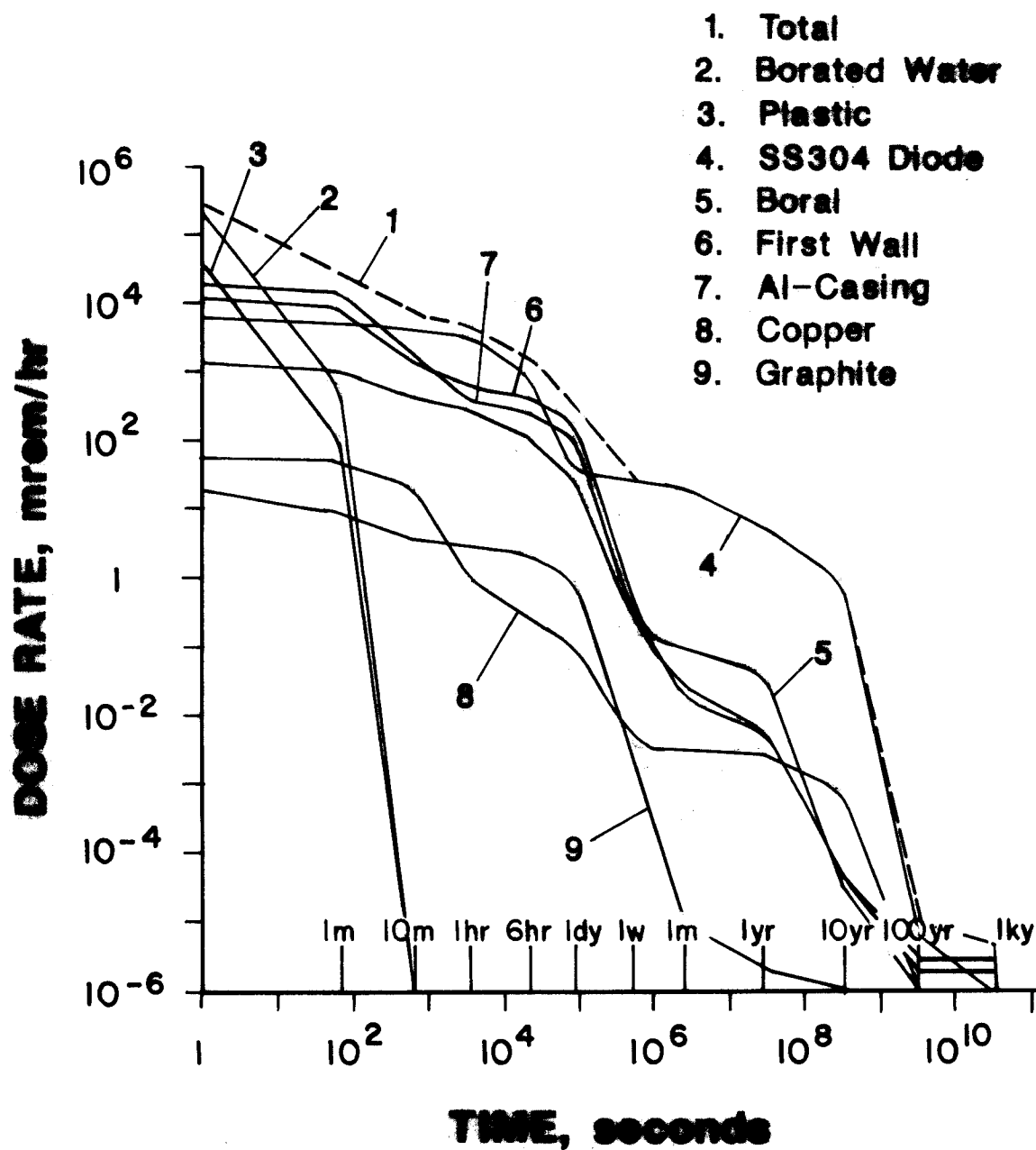


Fig. 13. Contributions from each component to the dose at the diode region for the 3 m chamber design.



It is therefore clear that the dose at the diode is dominated by the borated water and plastic activation at short times following shutdown and by the activation of first wall, boral and diode casing at intermediate times. The long term dose is mainly due to activation of the steel in the diode. This explains the results of Fig. 11 which show the dose at the diode to be higher for the 1 m chamber case than the 3 m chamber case at short times following shutdown. This is due to the fact that more borated water is used in the 1 m chamber case. At intermediate times after shutdown, the dose rate for the 1 m chamber case is about a factor of 3 lower than that for the 3 m chamber case, because of the additional shielding between the Al first wall and the diode that provides some attenuation for the decay gammas produced in the first wall and the neutrons that activate the Al diode casing. At long times following shutdown, the dose is dominated by the activity produced in the steel diode which is not very much affected by the additional shield used in the 1 m chamber case since a large part of the diode is in direct line of sight of source neutrons. Hence, using the 1 m chamber results only is a modest drop in the dose rate at long times after shutdown.

#### 4. SUMMARY

The neutronics, radioactivity and dose rate calculations for the Light Ion Fusion Target Development Facility have been performed. The biological dose rates were computed behind the first wall and at a point external to the diode casing following an operational period of one month. Two different chamber designs, 1 m and 3 m, were examined. The primary first wall and the diode material considered were Al-6061-T6 and SS304LN, respectively. The penetration through the wall to the diode has been taken as 10 cm in radius. Different shield materials were considered in the space between the 1 m chamber and the diodes. These included borated water, graphite and concrete. Using borated water resulted in the lowest dose rate in the diode region one week after shutdown. At this time the dose rate at the outer surface of the diode casing is 3.7 mrem/hr which is lower than the 24.5 mrem/hr dose rate obtained for the 3 m chamber design. On the other hand, the dose rate behind the Al first wall in the 1 m chamber design is 8.4 rem/hr one week after shutdown which is much larger than the 34.5 mrem/hr value obtained in the 3 m chamber design. All components of the facility contribute to the dose level measured at the vicinity of the diode significantly up to 1 week following shutdown but only the diode material (SS304LN) contributes significantly to the dose level after that time. The low dose rate in the diode region for the 1 m chamber design implies that hands-on maintenance of the diode might be possible. However, remote handling of the stainless steel diode is necessary in the 3 m chamber design. Once the diode has been remotely removed, manual access to the diode casing is possible at 1 week after shutdown.

#### Acknowledgements

Support for this work has been provided by the U.S. Department of Energy through Sandia National Laboratories. Computer support has been provided by the National Science Foundation through the San Diego Supercomputer Center.

## **APPENDIX A**

*The appendix contains the composition of the various materials used for the chamber wall and diode neutron transport and dose rate calculation.*

Table A.1. Chamber Wall Constituent Densities

2-1/4 Cr-1 Mo Steel		Aluminum-6061-T6	
Element	Density [atoms/b-cm]	Element	Density [atoms/b-cm]
C	$4.3135 \times 10^{-4}$	Mg	$6.6889 \times 10^{-4}$
Si	$6.7080 \times 10^{-4}$	Al	$5.8192 \times 10^{-2}$
P	$3.0413 \times 10^{-5}$	Si	$3.4741 \times 10^{-4}$
S	$2.9379 \times 10^{-5}$	Ti	$5.0925 \times 10^{-5}$
Ti	$2.9499 \times 10^{-5}$	Cr	$9.3827 \times 10^{-5}$
V	$2.7737 \times 10^{-5}$	Mn	$4.4401 \times 10^{-5}$
Cr	$1.9928 \times 10^{-3}$	Fe	$2.0383 \times 10^{-4}$
Mn	$4.2866 \times 10^{-4}$	Cu	$7.6781 \times 10^{-5}$
Fe	$8.0452 \times 10^{-2}$	Zn	$6.2193 \times 10^{-5}$
Cu	$1.4825 \times 10^{-4}$		
Mo	$4.9093 \times 10^{-4}$		

Table A.2. Composition of Materials Comprising the Diode, First Wall,  
Boral, and Graphite Moderator Regions

Element (wt.%)	Oxygen Free-High Conductivity Copper $\rho = 8.96 \text{ g/cm}^3$	SS304LN (Diode Material) $\rho = 8.03 \text{ g/cm}^3$	Al-6061-T6 (Chamber Wall) $\rho = 2.7 \text{ g/cm}^3$
H	0.0002	---	---
B	---	---	---
C	---	0.022	---
N	---	0.149	---
O	0.0003	---	---
Mg	---	---	1.0
Al	---	---	96.55
Si	---	0.62	0.60
P	0.0003	0.019	---
S	0.002	0.005	---
Ti	---	--	0.15
V	---	---	---
Cr	---	18.31	0.30
Mn	0.00004	1.33	0.15
Fe	0.001	69.73	0.70
Co	---	0.19	---
Ni	0.0013	9.30	---
Cu	99.9905	0.16	0.30
Zn	0.001	---	0.25
As	0.0003	---	---
Mo	---	0.17	---
Ag	0.0025	---	---
Cd	0.0001	---	---
Sn	0.0003	---	---
Sb	0.0008	---	---
Te	0.0002	---	---
Pb	0.0008	---	---

Table A.2. (continued)

Element (wt.%)	Boral			
	Graphite H-451 $\rho = 1.74 \text{ g/cm}^3$	(Enriched with B <sup>10</sup> ) $\rho = 2.53 \text{ g/cm}^3$	Plastic $\rho = 0.95 \text{ g/cm}^3$	Lithium $\rho = 0.534 \text{ g/cm}^3$
H	---	---	8.16	---
Li	---	---	---	100
B	---	16.8	---	---
C	100	4.9	48.64	---
O	---	---	43.20	---
Al	---	78.2	---	---

Table A.3. Composition of Shield Materials: Borated Water, Concrete and Graphite

Element (wt.%)	Borated Water $\rho = 2.53 \text{ g/cm}$	Concrete $\rho =$	Graphite $\rho = 1.74 \text{ g/cm}$
	Density [atoms/b-cm]		
H	6.85 e-02	1.24 e-02	---
Al	---	9.28 e-04	---
O	3.50 e-02	3.91 e-02	---
Fe	---	6.95 e-03	---
Mn	---	3.13 e-05	---
Ti	---	1.27 e-05	---
B-10	4.42 e-04	---	---
B-11	4.91 e-05	---	---
K	---	2.33 e-05	---
Ca	---	6.96 e-03	---
Na	---	2.22 e-04	---
Mg	---	7.40 e-04	---
N	---	8.70 e-06	---
S	---	6.44 e-05	---
C	---	5.68 e-03	8.73 e-02

## REFERENCES

1. D.L. Henderson, G.A. Moses, R.R. Peterson, "One-Dimensional Activation and Radiological Dose Calculations for the Light Ion Fusion Target Development Facility," University of Wisconsin Fusion Technology Institute Report UWFD-636 (1985).
2. R.D. O'Dell et al., "User's Manual for ONEDANT: A Code Package for One-Dimensional, Diffusion-Accelerated, Neutral-Particle Transport," LA-9184-M, Los Alamos National Laboratory (Feb. 1982).
3. R. MacFarlane, "Nuclear Data Libraries from Los Alamos for Fusion Neutronics Calculations," Trans. Am. Nucl. Soc. 46, 271(1984).
4. R. Alcouffe et al., "Users Guide for TWODANT: A Code Package for Two-Dimensional, Diffusion-Accelerated, Neutral-Particle Transport," LA-10049-M, Los Alamos National Laboratory (March 1984).
5. D.L. Henderson and O. Yasar, "DKR-ICF: A Radioactivity and Dose Rate Calculation Code Package," University of Wisconsin Fusion Technology Institute Report UWFD-714 (1986).
6. M.A. Gordinier and R.J. Howerton, "ACTL: Evaluated Neutron Activation Cross Section Library Evaluation Techniques and Reaction Index," UCRL-50400, Vol. 18 (1978).
7. C.M. Lederer et al., Table of Isotopes, Sixth and Seventh Editions, Wiley (1967 and 1978).
8. D.L. Henderson, M.E. Sawan, G.A. Moses, "Radiological Dose Calculations for the Diode Region of the Light Ion Fusion Target Development Facility," University of Wisconsin Fusion Technology Institute Report UWFD-707 (1986).